

Second-Moment Budgets and Mixing Intensity in the Stably Stratified Atmospheric Boundary Layer over Thermally Heterogeneous Surfaces

DMITRII V. MIRONOV

German Weather Service, Offenbach am Main, Germany

PETER P. SULLIVAN

National Center for Atmospheric Research, Boulder, Colorado*

(Manuscript received 6 March 2015, in final form 20 September 2015)

ABSTRACT

The effect of horizontal temperature heterogeneity of the underlying surface on the turbulence structure and mixing intensity in the stably stratified boundary layer (SBL) is analyzed using large-eddy simulation (LES). Idealized LESs of flows driven by fixed winds and homogeneous and heterogeneous surface temperatures are compared. The LES data are used to compute statistical moments, to estimate budgets of the turbulence kinetic energy (TKE), of the temperature variance and of the temperature flux, and to assess the relative importance of various terms in maintaining the budgets. Unlike most previous studies, the LES-based second-moment budgets are estimated with due regard for the subgrid-scale contributions.

The SBL over a heterogeneous surface is more turbulent with larger variances (and TKE), is better vertically mixed, and is deeper compared to its homogeneous counterpart. The most striking difference between the cases is exhibited in the temperature variance and its budget. Because of surface heterogeneity, the turbulent transport term (divergence of the third-order moment) not only redistributes the temperature variance vertically but is a net gain. The increase in the temperature variance near the heterogeneous surface explains the reduced magnitude of the downward buoyancy flux and the ensuing increase in TKE that leads to more vigorous mixing. Analysis of the temperature flux budget shows that the transport term contributes to net production/destruction. Importantly, the role of the third-order transport cannot be elucidated if the budgets are computed based solely on resolved-scale fields. Implications for modeling (parameterizing) the SBL over thermally heterogeneous surfaces are discussed.

1. Introduction

Representation of stably stratified boundary layer turbulence in numerical models of atmospheric circulation is one of the key unresolved issues that slows down progress in climate modeling, numerical weather prediction, and related applications. Turbulence in a stably stratified boundary layer (SBL) is weak and often intermittent in space and time. It responds to various effects, for example, internal gravity waves, cold-air meandering, and

horizontal inhomogeneity of the underlying surface (e.g., [Mahrt 2014](#)). Current SBL models (parameterization schemes), used in numerical weather prediction, climate studies, and related applications do not include these important effects in a physically sound way.

The majority of SBL turbulence models are based on truncated budget equations for the second-order moments of fluctuating fields. Despite their fundamental importance (see discussion in [Mironov 2009](#)), the second-moment budgets in the SBL have not been systematically analyzed so far. In most large-eddy simulation (LES) and direct numerical simulation (DNS) studies performed to date, the emphasis is on the turbulence kinetic energy (TKE) budget (e.g., [Coleman et al. 1992](#); [Brown et al. 1994](#); [Kosović and Curry 2000](#); [Saiki et al. 2000](#); [Jiménez and Cuxart 2005](#); [van Dop and Axelsen 2007](#); [Taylor and Sarkar 2008](#); [Huang and Bou-Zeid 2013](#); [Ansorge and Mellado](#)

*The National Center for Atmospheric Research is sponsored by the National Science Foundation.

Corresponding author address: Dmitrii V. Mironov, Deutscher Wetterdienst, FE14, Frankfurter Str. 135, D-63067 Offenbach am Main, Germany.
E-mail: dmitrii.mironov@dwd.de

2014). Very few attempts have been made to analyze other second-moment budgets, such as the budget of temperature variance (e.g., Mason and Derbyshire 1990) and of vertical scalar flux and Reynolds-stress components (e.g., Andr n 1995). It should also be noted that the LES-based second-moment budgets are often estimated on the basis of resolved-scale fields only. However, the subgrid-scale (SGS) contributions may be substantial, particularly in the SBL, and should be retained in order to close the second-moment budgets to a good order. In the present study, the budgets of TKE, of the potential temperature variance, and of the vertical and horizontal components of the potential temperature flux are computed with due regard for the SGS contributions to the various budget terms, using a dataset generated by LES.

Another important aspect of the SBL that is not yet satisfactorily understood is how surface heterogeneity (e.g., with respect to the temperature) modifies the structure and the transport properties of SBL turbulence. Stoll and Port -Agel (2009) performed LESs of SBL over thermally homogeneous surfaces and over thermally heterogeneous surfaces where spanwise homogeneous surface temperature patches alternate between two temperature values but the horizontal-mean surface temperature is the same as in homogeneous runs. They found, among other things, that the heterogeneous SBL is more turbulent and is better vertically mixed with respect to mean potential temperature. We attempt to explain the enhanced vertical mixing in the SBL over thermally heterogeneous surface through a comparative analysis of the second-moment budgets in homogeneous and heterogeneous SBLs. It should be mentioned that the SBLs with weak-to-moderate static stability are considered in what follows. Strongly stable boundary layers are beyond the scope of the present study.

Section 2 describes the simulations performed. In section 3, vertical profiles of mean fields and second-order moments (fluxes and variances) are discussed. Section 4 presents a comparative analysis of the second-order moment budgets in the homogeneous and heterogeneous SBLs. A procedure to compute LES-based approximations of the ensemble-mean second-moment budgets with due regard for the SGS contributions is outlined; budgets of the TKE, of the potential temperature variance, and of the potential temperature flux are analyzed; and a rational explanation of the enhanced vertical mixing in the heterogeneous SBL is suggested. Results from the analysis, their implications for modeling (parameterizing) horizontally heterogeneous SBLs in large-scale atmospheric models, and some critical issues related to the LES of

stably stratified heterogeneous flows are discussed in section 5. Conclusions are presented in section 6.

We use standard notation, where t is time, x_i represents the right-hand Cartesian coordinates, u_i represents the velocity components, θ is the potential temperature (for the sake of brevity, it will also be referred to as simply “temperature”), p is the kinematic pressure (the pressure deviation from the hydrostatically balanced pressure divided by the constant reference density ρ_r), f_i is the Coriolis parameter, $\beta_i = -g_i/\theta_r$ is the buoyancy parameter, g_i is the acceleration due to gravity, and θ_r is the constant reference value of temperature (the Boussinesq approximation is used, which is an accurate approximation for the lower troposphere). The Einstein summation convention for repeated indices is adopted. An overbar denotes a resolved-scale (filtered) variable computed by a large-eddy model. In section 4a, where the LES-based budget equations for the second-order moments are derived, the angle brackets denote a horizontal mean, and a double prime denotes a deviation from the mean. In the rest of the paper, the angle brackets denote the quantities obtained on the basis of LES data by averaging over horizontal planes and over time.

2. LES dataset

The LES code used in the present study is described in detail in Moeng (1984), Moeng and Wyngaard (1988), Sullivan et al. (1994, 1996), and Sullivan and Patton (2008, 2011). A description of the code is not repeated here; readers are referred to the above papers. However, the salient features of the SGS model deemed pertinent to the simulated flows (the structure of which is complicated by the stable buoyancy stratification and, in one case, by the heterogeneity of the underlying surface) are briefly outlined below.

The residual-stress tensor $\tau_{ij} = \overline{u_i u_j} - \overline{u_i} \overline{u_j}$ (which will be referred to, albeit somewhat loosely, as “the SGS stress tensor” in what follows)¹ and the residual (SGS) temperature flux $\tau_{i\theta} = \overline{u_i \theta} - \overline{u_i} \overline{\theta}$ are determined through downgradient formulations. We use the Lilly (1967) notation with no primes to emphasize that the filter operator used to derive the governing equations of a large-eddy model does not generally satisfy the Reynolds averaging assumption. The deviatoric part of τ_{ij} , that is, $\tau_{ij} - (2/3)\delta_{ij}e$, with $e = \tau_{ii}/2$ being the SGS TKE, and $\tau_{i\theta}$ are related to (twice) the strain rate and

¹Strictly speaking, the stress tensor is $-\rho\tau_{ij}$, ρ being the fluid density. See, for example, Pope (2000).

to the temperature gradient, respectively, through the scalar SGS eddy diffusion coefficients for momentum K_M and heat K_H . The SGS eddy diffusivities are computed from $K_M = \text{Pr}K_H = C_K l e^{1/2}$, where Pr is the SGS Prandtl number, and C_K is a dimensionless constant [estimates of this and the other model constants/parameters are given in Sullivan et al. (1994)]. In unstable and neutral stratification, the SGS mixing length l is equal to the effective mesh size, $l = \Delta = [(9/4)\Delta_1\Delta_2\Delta_3]^{1/3}$, where Δ_1 , Δ_2 , and Δ_3 are the mesh sizes in x_1 , x_2 , and x_3 directions, respectively, and the factor 9/4 appears because of dealiasing of the upper 1/3 of wavenumbers in the horizontal directions. In stable stratification, the mixing length is reduced with due regard for the effect of buoyancy, $l = \min(\Delta, C_B e/N)$, where N is the buoyancy frequency, and C_B is a dimensionless constant. Following Deardorff (1980), Pr is taken to be stability dependent, $\text{Pr}^{-1} = 1 + 2l/\Delta$. The SGS TKE is determined from its transport equation, where the turbulent transport term (the sum of the third-order velocity correlation $T_{ijj}/2$ and the pressure-velocity correlation $\overline{u_i p} - \overline{u_i} \overline{p}$; see section 4a for notation) is parameterized through a downgradient diffusion formulation, $(1/2)T_{ijj} + \overline{u_i p} - \overline{u_i} \overline{p} = -2K_m \partial e / \partial x_i$, and the TKE dissipation rate ε is computed from $\varepsilon = C_\varepsilon e^{3/2}/l$, C_ε being a dimensionless constant. The Monin–Obukhov surface-layer flux–profile relationships are applied locally, that is, point by point in the LES (cf. Stoll and Porté-Agel 2009). The surface fluxes for each model grid box are computed using the surface temperature and the temperature and velocity at the first model level above the ground. This is a departure from the Sullivan et al. (1994) two-part model that applies the Monin–Obukhov similarity relations in the horizontal-mean sense close to the surface and recovers local downgradient formulations for fluxes away from the surface. With the local application of the surface-layer flux–profile relationships, the two-part model essentially reduces to the baseline model [see Sullivan et al. (1994) for a detailed description of both models]. Note that the local use of the surface-layer flux–profile relationships is a sensible and pragmatic recipe to compute the surface fluxes in LES (the use of the Monin–Obukhov similarity in the horizontal-mean sense over a thermally heterogeneous surface is simply incorrect). The issue is discussed in section 5.

Using the basic GEWEX Atmospheric Boundary Layer Study (GABLS) simulation (Beare et al. 2006) as a reference, one SBL flow with the thermally homogeneous underlying surface (case HOM) and one flow with the thermally heterogeneous surface (case HET) are generated. In both simulations, the number of grid points is 200, 200, and 192 in the streamwise

x_1 , spanwise x_2 , and vertical x_3 directions, respectively, and the numerical domain size is 400 m in all directions. Potential temperature is the only thermodynamic variable that affects the distribution of buoyancy. The x_3 axis (directed upward), the vector of gravity, and the angular velocity of the reference-frame rotation are aligned. Then the only nonzero components of the Coriolis parameter and of the buoyancy parameter are, respectively, $f_3 = 1.39 \times 10^{-4} \text{ s}^{-1}$ and $\beta_3 = -g_3/\theta_r$, where $g_3 = -9.81 \text{ m s}^{-2}$ and $\theta_r = 265 \text{ K}$. The flows are driven by a constant streamwise geostrophic wind $U_g = 8.0 \text{ m s}^{-1}$; the spanwise geostrophic wind V_g is zero. The surface roughness length for both wind and temperature is $z_0 = 0.1 \text{ m}$.

In both simulated cases, periodic boundary conditions are applied in the x_1 and x_2 horizontal directions. At the upper boundary of the numerical domain, zero SGS TKE, free slip for the horizontal velocity components, the potential temperature gradient $\Gamma_\theta = 10^{-2} \text{ K m}^{-1}$, and the radiative boundary conditions that allow internal gravity waves to leave the system are applied. At the underlying surface, Dirichlet boundary conditions are adopted for both velocity and temperature; all three components of the velocity vector are set to zero, and the surface temperature is determined by a prescribed surface cooling rate. The vertical fluxes of horizontal momentum and of heat (temperature) are evaluated from the surface layer similarity that is applied locally.

The time-varying surface temperature is determined by a specified surface cooling rate. In the homogeneous case, a constant cooling rate $R_c = -0.375 \text{ K h}^{-1}$ is applied over the first 8 h of the simulations. Note that in the original GABLS simulation of Beare et al. (2006) a cooling rate of -0.25 K h^{-1} was used; thus the present case is more strongly stratified. In the heterogeneous case, the cooling rate is constant in the spanwise direction and varies sinusoidally in the streamwise direction as $(\partial\theta/\partial t)_{\text{sfc}} = R_c[1 + \sin(4\pi x_1/L_1)]$, where L_1 is the domain size in the x_1 direction. The horizontal-mean surface temperature is the same as in the homogeneous case. Eight hours of cooling lead to a surface temperature difference of 6 K between the warm and the cold stripes. Following this initial 8-h period, both simulations are continued, using a constant cooling rate R_c . The setup of our heterogeneous simulation is broadly similar to that of Stoll and Porté-Agel (2009), differing in the magnitude of the surface cooling rate and the shape of the surface temperature heterogeneity patterns (a series of spanwise homogeneous surface temperature patches that alternate between two temperature values in the simulations of Stoll and Porté-Agel versus a

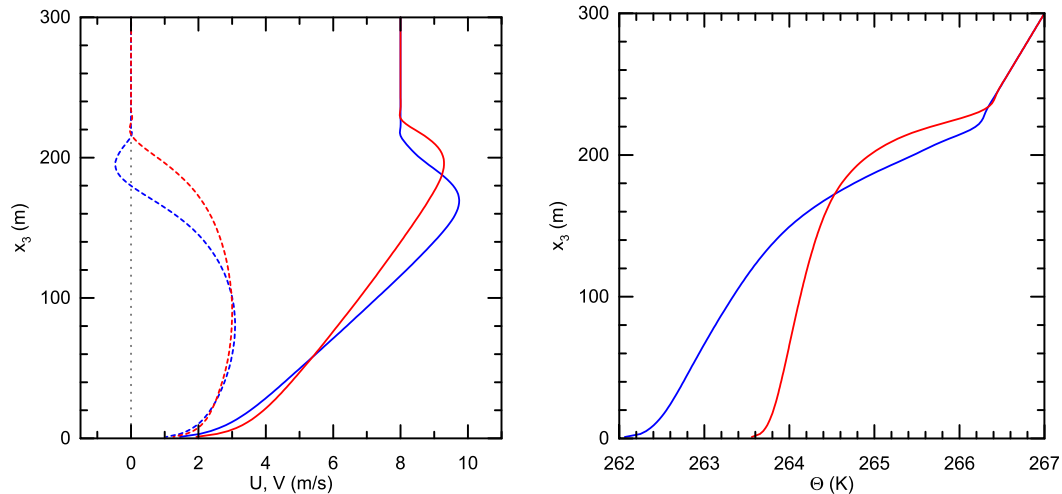


FIG. 1. (left) Streamwise (solid curves) and spanwise (dashed curves) components of mean wind, and (right) mean temperature from simulations HOM (blue) and HET (red).

sinusoidal variation of the surface temperature in the present simulations).

The initial temperature profile has a two-layer structure. A layer of depth $h_i = 100$ m and depth-constant temperature $\bar{\theta} = \theta_r$ is capped by a stratified layer where the temperature increases linearly at a rate Γ_θ . The initial velocity components \bar{u}_2 and \bar{u}_3 in the spanwise and vertical direction, respectively, are zero throughout the domain. The initial streamwise velocity component \bar{u}_1 is set equal to U_g . To facilitate the growth of turbulence, small random disturbances are added to the initial temperature and velocity fields in the lower part of the domain ($x_3 < h_i$), and the SGS TKE there is set to a small value.

To obtain approximations to ensemble-mean quantities, the LES data are averaged over horizontal planes, and the resulting profiles are then averaged over several thousand time steps. The number of samples varies between the two cases, but the sampling time covers the last 1.75 h of simulations.

3. Mean fields and second-order moments

Vertical profiles of the streamwise $U = \langle \bar{u}_1 \rangle$ and the spanwise $V = \langle \bar{u}_2 \rangle$ mean wind components and of mean temperature $\Theta = \langle \bar{\theta} \rangle$ are shown in Fig. 1. A comparison of cases HOM and HET suggests that in the latter the SBL is deeper. The components of mean wind are quite similar in shape in both cases (except for V near the boundary layer top), whereas the mean temperature profiles are essentially different. The SBL over a thermally heterogeneous surface is much better vertically mixed with respect to Θ . The results

shown in Fig. 1 confirm previous findings of Stoll and Porté-Agel (2009).

Figure 2 shows vertical profiles of the streamwise $UW = \langle \bar{u}_1' \bar{u}_3' \rangle + \langle \tau_{13} \rangle$ and spanwise $VW = \langle \bar{u}_2' \bar{u}_3' \rangle + \langle \tau_{23} \rangle$ momentum flux components and vertical temperature flux $WT = \langle \bar{u}_3' \bar{\theta}'' \rangle + \langle \tau_{3\theta} \rangle$. The SGS stress τ_{ij} and the SGS temperature flux $\tau_{i\theta}$ are computed by the SGS model. In the heterogeneous case, the magnitude of the downward temperature (heat) flux is reduced over most of the boundary layer. The magnitude of the downward momentum flux is increased, but the effect is not as strong as for the vertical temperature flux (cf. the profiles of mean temperature and mean wind components).

Vertical profiles of horizontal components of the temperature flux $UT = \langle \bar{u}_1' \bar{\theta}'' \rangle + \langle \tau_{1\theta} \rangle$ and $VT = \langle \bar{u}_2' \bar{\theta}'' \rangle + \langle \tau_{2\theta} \rangle$ are shown in Fig. 3. The magnitude of both streamwise and spanwise temperature flux components is reduced in the heterogeneous case over most of the SBL (except near the boundary layer top).

Figure 4 shows vertical profiles of the turbulence kinetic energy $TKE = (1/2) \langle \bar{u}_i'^2 \rangle + \langle e \rangle$ and of the velocity variances $UU = \langle \bar{u}_1'^2 \rangle + \langle \tau_{11} \rangle$ (streamwise), $VV = \langle \bar{u}_2'^2 \rangle + \langle \tau_{22} \rangle$ (spanwise), and $WW = \langle \bar{u}_3'^2 \rangle + \langle \tau_{33} \rangle$ (vertical). The velocity variances and, hence, the TKE are larger in the heterogeneous case. The SGS TKE e is a small portion of the total (resolved + SGS) TKE, indicating that turbulence in the SBL in our simulations is well resolved.

The temperature variance $TT = \langle \bar{\theta}''^2 \rangle + \langle \vartheta \rangle$ shown in Fig. 5 reveals the most striking difference between HOM and HET. Note that, unlike the SGS TKE, the SGS temperature variance $\vartheta = \bar{\theta}''^2 - \bar{\theta}''^2$ is not computed by the SGS model. It is estimated as (Nieuwstadt et al. 1993; Heinze et al. 2015) $\vartheta = 5\tau_{i\theta}^2/e$, where the numerical

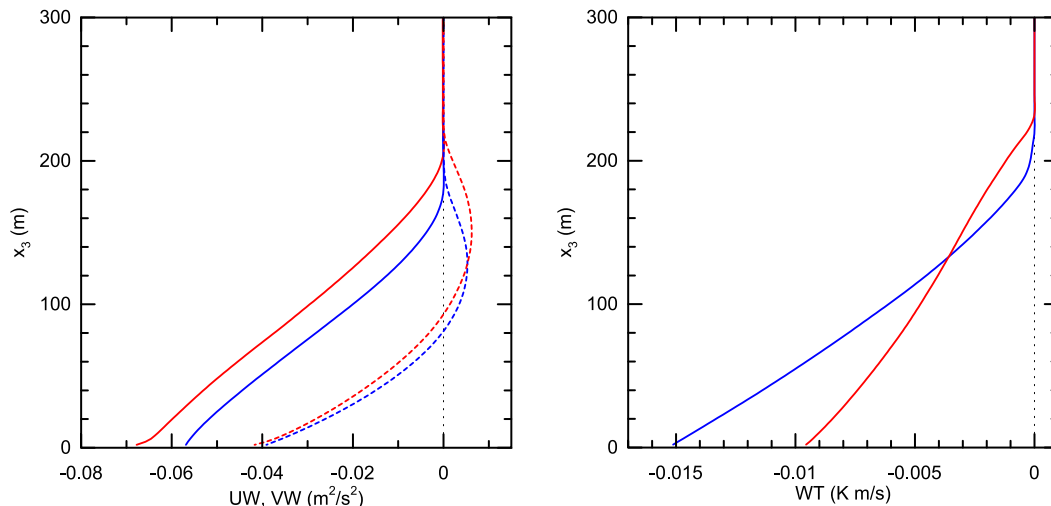


FIG. 2. (left) Streamwise (solid curves) and spanwise (dashed curves) momentum flux components, and (right) vertical component of the temperature flux from simulations HOM (blue) and HET (red).

value of the coefficient follows from the consideration of the inertial subrange temperature spectrum (Moeng and Wyngaard 1988; Peltier and Wyngaard 1995). In the heterogeneous case, TT has a distinct maximum near the SBL top, apparently because of an increased mean temperature gradient and, hence, an increased temperature variance production. The most pronounced difference between HOM and HET is close to the surface, where the temperature variance is much larger in the heterogeneous case. This increase in the temperature variance helps explain the reduced magnitude of the downward temperature flux, the increased TKE, and more vigorous vertical mixing in the heterogeneous SBL. The issue is discussed below in more detail in the

context of comparative analysis of the second-moment budgets.

4. Second-order moment budgets

a. Estimation of second-order moment budgets using LES data

In this section, we explain how approximations to the ensemble-mean budget equations for the second-order moments are obtained from numerical data generated with an LES. It should be borne in mind that the second-moment budgets derived from LES are not the same as the ensemble-mean budgets. The relation between the

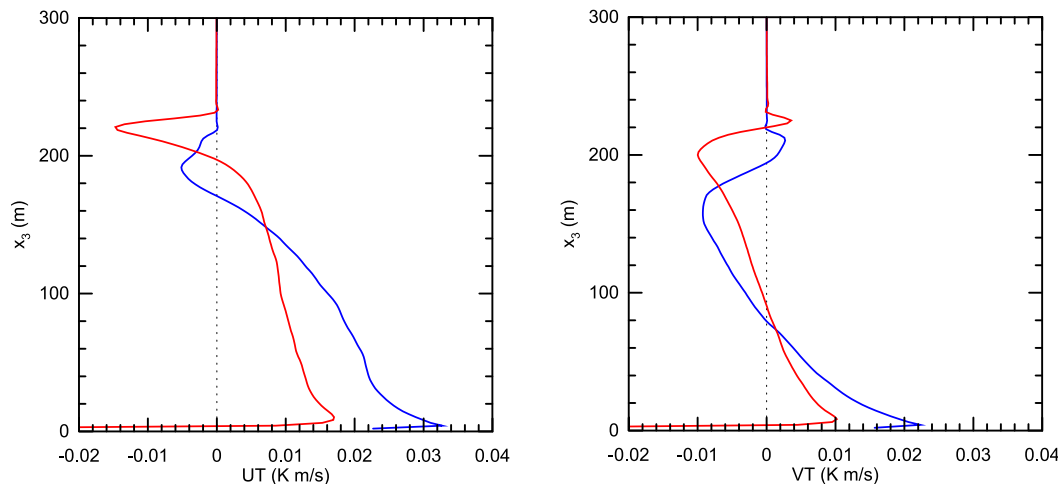


FIG. 3. (left) Streamwise and (right) spanwise components of the temperature flux from simulations HOM (blue) and HET (red).

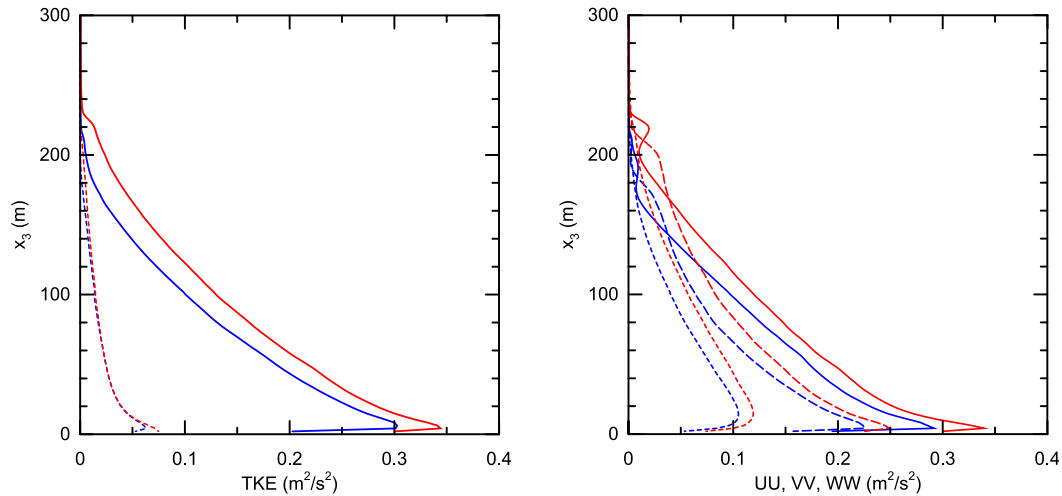


FIG. 4. (left) Total (solid curves) and SGS (dashed curves) turbulence kinetic energy, and (right) streamwise (solid curves), spanwise (long-dashed curves), and vertical (short-dashed curves) velocity variances from simulations HOM (blue) and HET (red).

two sets of budget equations is not entirely straightforward, and the approach used by various authors is not always made clear.

Consider the budget of the temperature variance. We “forget” for the moment that the averaging denoted by angle brackets is averaging over the horizontal (in this section only; in the rest of the paper, angle brackets denote the quantities averaged horizontally and over time) that makes a number of terms in the second-moment budgets disappear. The temperature variance budget equation is first presented in its full three-dimensional form. Then it is simplified by taking the properties of the horizontal averaging into account.

The budget equation for the resolved-scale temperature variance $\langle \bar{\theta}''^2 \rangle$ is obtained from the filtered temperature equation in the following way (e.g., Deardorff 1974b; Mironov et al. 2000; Heinze et al. 2015). Subtracting from the transport equation for $\bar{\theta}$, its horizontal mean yields the equation for $\bar{\theta}''$. Multiplying that equation by $\bar{\theta}''$ and averaging the result yields the equation for $\langle \bar{\theta}''^2 \rangle$. It reads

$$\begin{aligned} & \frac{1}{2} \left(\frac{\partial}{\partial t} + \langle \bar{u}_i \rangle \frac{\partial}{\partial x_i} \right) \langle \bar{\theta}''^2 \rangle \\ &= - \langle \bar{u}_i'' \bar{\theta}'' \rangle \frac{\partial \langle \bar{\theta} \rangle}{\partial x_i} - \frac{1}{2} \frac{\partial}{\partial x_i} \langle \bar{u}_i'' \bar{\theta}''^2 \rangle - \left\langle \bar{\theta}'' \frac{\partial \tau''_{i\theta}}{\partial x_i} \right\rangle. \end{aligned} \quad (1)$$

The first two terms on the right-hand side (rhs) of Eq. (1) represent the effects of the mean-gradient production/destruction and of the turbulent transport of the resolved-scale temperature variance, respectively. The

physical meaning of the last term on the rhs is discussed below. Recall that the filtered equations used by a large-eddy model do not contain molecular terms. As a result, the equations for the resolved-scale second-order moments do not contain molecular destruction terms.

The averaged budget equation for the SGS temperature variance ϑ reads [see Lilly (1967) and Deardorff (1973), where the transport equations for the SGS quantities are considered in detail]

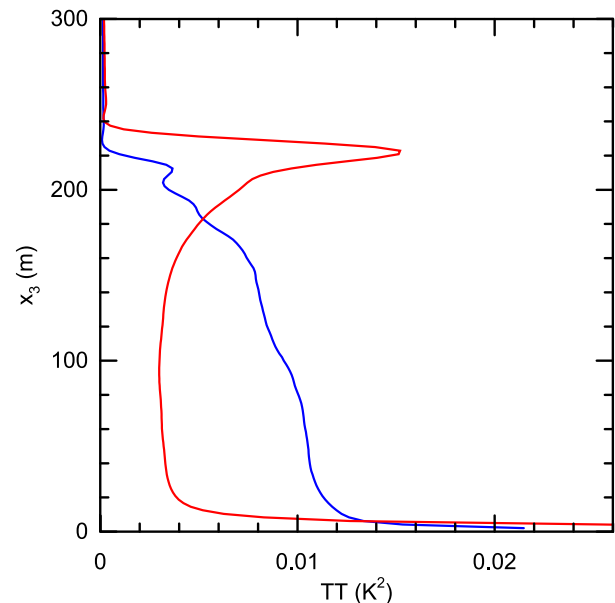


FIG. 5. Temperature variance from simulations HOM (blue) and HET (red).

$$\begin{aligned} & \frac{1}{2} \left(\frac{\partial}{\partial t} + \langle \bar{u}_i \rangle \frac{\partial}{\partial x_i} \right) \langle \vartheta \rangle \\ &= - \left\langle \tau_{i\theta} \frac{\partial \bar{\theta}}{\partial x_i} \right\rangle - \frac{1}{2} \frac{\partial}{\partial x_i} (\langle \bar{u}_i'' \vartheta'' \rangle + \langle T_{i\theta} \rangle) - \langle \varepsilon_\theta \rangle, \end{aligned} \quad (2)$$

where $T_{i\theta} = \bar{u}_i \theta^2 - \bar{u}_i \bar{\theta}^2 + 2(\bar{u}_i \bar{\theta}^2 - \bar{u}_i \bar{\theta} \bar{\theta})$ is the SGS triple correlation (SGS flux of ϑ), and ε_θ is the temperature variance dissipation rate.

The first term on the rhs of Eq. (2) is rearranged to give

$$- \left\langle \tau_{i\theta} \frac{\partial \bar{\theta}}{\partial x_i} \right\rangle = - \langle \tau_{i\theta} \rangle \frac{\partial \langle \bar{\theta} \rangle}{\partial x_i} - \frac{\partial}{\partial x_i} \langle \bar{\theta}'' \tau_{i\theta}'' \rangle + \left\langle \bar{\theta}'' \frac{\partial \tau_{i\theta}''}{\partial x_i} \right\rangle. \quad (3)$$

Substituting Eq. (3) into Eq. (2), we obtain

$$\begin{aligned} \frac{1}{2} \left(\frac{\partial}{\partial t} + \langle \bar{u}_i \rangle \frac{\partial}{\partial x_i} \right) \langle \vartheta \rangle &= - \langle \tau_{i\theta} \rangle \frac{\partial \langle \bar{\theta} \rangle}{\partial x_i} - \frac{1}{2} \frac{\partial}{\partial x_i} (\langle \bar{u}_i'' \vartheta'' \rangle \\ &+ 2 \langle \bar{\theta}'' \tau_{i\theta}'' \rangle + \langle T_{i\theta} \rangle) - \langle \varepsilon_\theta \rangle \\ &+ \left\langle \bar{\theta}'' \frac{\partial \tau_{i\theta}''}{\partial x_i} \right\rangle, \end{aligned} \quad (4)$$

where the first and the second terms on the rhs of Eq. (4) represent the mean-gradient production/destruction and the transport of the SGS temperature variance, respectively. These terms are similar in nature to the first and the second terms, respectively, on the rhs of Eq. (1) for the resolved-scale temperature variance. The last term on the rhs of Eq. (4) is equal in magnitude but opposite in sign to the last term on the rhs of Eq. (1). It may be referred to as the scale interaction term that describes the transfer of the temperature variance between the resolved and the subgrid scales. Clearly, this term disappears if the total (i.e., resolved + SGS) temperature variance is considered.

Adding Eqs. (1) and (4) yields the budget equation for the total temperature variance $\langle \bar{\theta}''^2 \rangle + \langle \vartheta \rangle$. It reads

$$\begin{aligned} \frac{\partial}{\partial t} \left(\frac{1}{2} \langle \bar{u}_i''^2 \rangle + \langle e \rangle \right) &= - \left[(\langle \bar{u}_1'' \bar{u}_3'' \rangle + \langle \tau_{13} \rangle) \frac{\partial \langle \bar{u}_1 \rangle}{\partial x_3} + (\langle \bar{u}_2'' \bar{u}_3'' \rangle + \langle \tau_{23} \rangle) \frac{\partial \langle \bar{u}_2 \rangle}{\partial x_3} \right] + \beta_3 (\langle \bar{u}_3'' \bar{\theta}'' \rangle + \langle \tau_{3\theta} \rangle) - \langle \varepsilon \rangle \\ &- \frac{\partial}{\partial x_3} \left(\frac{1}{2} \langle \bar{u}_3'' \bar{u}_i''^2 \rangle + \langle \bar{u}_3'' e'' \rangle + \langle \bar{u}_i'' \tau_{i3}'' \rangle + \langle \bar{u}_3'' \bar{p}'' \rangle + \frac{1}{2} \langle T_{3ii} \rangle + \langle \bar{u}_3 \bar{p} \rangle - \bar{u}_3 \bar{p} \right), \end{aligned} \quad (7)$$

$$\begin{aligned} \frac{\partial}{\partial t} (\langle \bar{u}_3'' \bar{\theta}'' \rangle + \langle \tau_{3\theta} \rangle) &= - (\langle \bar{u}_3''^2 \rangle + \langle \tau_{33} \rangle) \frac{\partial \langle \bar{\theta} \rangle}{\partial x_3} + \beta_3 (\langle \bar{\theta}''^2 \rangle + \langle \vartheta \rangle) - \left(\left\langle \bar{\theta}'' \frac{\partial \bar{p}''}{\partial x_3} \right\rangle + \left\langle \bar{\theta} \frac{\partial \bar{p}}{\partial x_3} - \bar{\theta} \frac{\partial \bar{p}}{\partial x_3} \right\rangle \right) - \frac{\partial}{\partial x_3} (\langle \bar{u}_3'' \bar{\theta}'' \rangle \\ &+ 2 \langle \bar{u}_3'' \tau_{3\theta}'' \rangle + \langle \bar{\theta}'' \tau_{33}'' \rangle + \langle T_{33\theta} \rangle), \end{aligned} \quad (8)$$

where $T_{3ii} = \bar{u}_3 \bar{u}_i^2 - \bar{u}_3 \bar{u}_i^2 + 2(\bar{u}_3 \bar{u}_i^2 - \bar{u}_i \bar{u}_i \bar{u}_3)$ and $T_{33\theta} = \bar{u}_3^2 \bar{\theta} - \bar{u}_3^2 \bar{\theta} + 2(\bar{u}_3^2 \bar{\theta} - \bar{u}_3 \bar{u}_3 \bar{\theta})$ are the third-order SGS transport terms. The terms on the rhs of Eq. (7)

$$\begin{aligned} & \frac{1}{2} \left(\frac{\partial}{\partial t} + \langle \bar{u}_i \rangle \frac{\partial}{\partial x_i} \right) (\langle \bar{\theta}''^2 \rangle + \langle \vartheta \rangle) \\ &= - (\langle \bar{u}_i'' \bar{\theta}'' \rangle + \langle \tau_{i\theta} \rangle) \frac{\partial \langle \bar{\theta} \rangle}{\partial x_i} - \langle \varepsilon_\theta \rangle - \frac{1}{2} \frac{\partial}{\partial x_i} (\langle \bar{u}_i'' \bar{\theta}''^2 \rangle \\ &+ \langle \bar{u}_i'' \vartheta'' \rangle + 2 \langle \bar{\theta}'' \tau_{i\theta}'' \rangle + \langle T_{i\theta} \rangle). \end{aligned} \quad (5)$$

The terms on the rhs of Eq. (5) are treated as approximations to the mean-gradient production/destruction, the dissipation, and the transport terms in the ensemble-mean temperature variance budget equation.

With due regard for the periodic boundary conditions in x_1 and x_2 horizontal directions and zero horizontal-mean vertical velocity $\langle \bar{u}_3 \rangle$, Eq. (5) is simplified to give the following temperature variance budget equation:

$$\begin{aligned} \frac{1}{2} \frac{\partial}{\partial t} (\langle \bar{\theta}''^2 \rangle + \langle \vartheta \rangle) &= - (\langle \bar{u}_3'' \bar{\theta}'' \rangle + \langle \tau_{3\theta} \rangle) \frac{\partial \langle \bar{\theta} \rangle}{\partial x_3} - \langle \varepsilon_\theta \rangle \\ &- \frac{1}{2} \frac{\partial}{\partial x_3} (\langle \bar{u}_3'' \bar{\theta}''^2 \rangle + \langle \bar{u}_3'' \vartheta'' \rangle \\ &+ 2 \langle \bar{\theta}'' \tau_{3\theta}'' \rangle + \langle T_{3\theta} \rangle). \end{aligned} \quad (6)$$

An approximation to the temperature variance dissipation rate is computed as (Moeng and Wyngaard 1989; Peltier and Wyngaard 1995; Heinze et al. 2015) $\langle \varepsilon_\theta \rangle = \langle K_H (\partial \bar{\theta} / \partial x_i)^2 \rangle$, where K_H is the SGS temperature conductivity. The SGS triple correlation term $\langle T_{3\theta} \rangle$ cannot be estimated from our LES data and is treated as part of the budget imbalance. It is presumably small (cf. Deardorff 1974a).

The budget equations for the Reynolds stress and for the temperature flux are derived in a similar way as the equation for the temperature variance. With due regard for the periodic boundary conditions in horizontal directions, the budget equations for the TKE (half the trace of the Reynolds-stress tensor) and for the vertical temperature flux read

represent the effects of the mean velocity shear, buoyancy, dissipation and turbulent transport (due to the third-order velocity correlations and the pressure-velocity

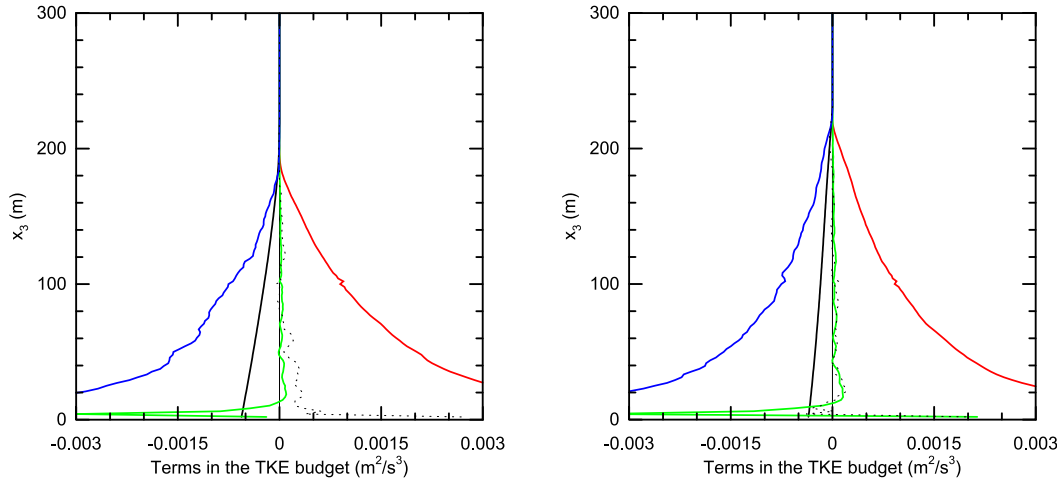


FIG. 6. TKE budget from simulations (left) HOM and (right) HET. Curves represent the effects of mean velocity shear (red), buoyancy (black), dissipation (blue), and the sum of third-order transport and pressure transport (green). Thin dotted black curves show the budget imbalance.

correlations), respectively. The terms on the rhs of Eq. (8) represent the effects of the mean temperature gradient, buoyancy, pressure gradient–temperature covariance, and turbulent transport, respectively.

An estimate of the TKE dissipation rate $\langle \varepsilon \rangle$ stems from the SGS TKE equation carried by the large-eddy model. The SGS contribution to the pressure gradient–temperature covariance (the SGS pressure-scrambling term) is computed as $\langle \overline{\theta \partial p / \partial x_3} - \overline{\theta \partial \overline{p} / \partial x_3} \rangle = -\langle \tau_{i\theta} \partial \overline{u}_3 / \partial x_i \rangle - \langle \tau_{3i} \partial \overline{\theta} / \partial x_i \rangle + \beta_3 \langle \vartheta \rangle$. This approximation is obtained from the truncated SGS temperature flux budget equation, assuming a steady-state balance between the mean-gradient, buoyancy, Coriolis, and pressure terms at the subgrid scales [see Mironov (2001) and Heinze et al. (2015) for details]. Results from previous studies (Khanna 1998; Mironov et al. 2000; Mironov 2001; Heinze et al. 2015) suggest that the SGS

pressure-scrambling term should be added to the resolved-scale pressure-scrambling term in order to close the temperature flux budget to a good order. The third-order SGS transport term $\mathcal{T}_{33\theta}$ in Eq. (8) cannot be estimated from our LES data, as this term is not computed within the SGS model. It is treated as part of the budget imbalance. In the SGS TKE equation, the sum of the SGS third-order transport term and the SGS pressure transport term is parameterized through the downgradient diffusion approximation (see section 2). Hence, the total SGS transport term, $(1/2)\mathcal{T}_{3ii} + \overline{u}_3 \overline{p} - \overline{u}_3 \overline{p}$, in Eq. (7) can be estimated, but it is impossible to discriminate between the third-order transport and the pressure transport of the SGS TKE by the SGS fluctuating motions.

The budget equation for the horizontal components of the temperature flux reads

$$\begin{aligned} \frac{\partial}{\partial t} (\langle \overline{u}_i'' \overline{\theta}'' \rangle + \langle \tau_{i\theta} \rangle) &= -(\langle \overline{u}_i'' \overline{u}_3'' \rangle + \langle \tau_{i3} \rangle) \frac{\partial \langle \overline{\theta} \rangle}{\partial x_3} - (\langle \overline{u}_3'' \overline{\theta}'' \rangle + \langle \tau_{3\theta} \rangle) \frac{\partial \langle \overline{u}_i \rangle}{\partial x_3} \\ &\quad - \varepsilon_{i3k} f_3 (\langle \overline{u}_k'' \overline{\theta}'' \rangle + \langle \tau_{k\theta} \rangle) - \left(\left\langle \overline{\theta}'' \frac{\partial \overline{p}''}{\partial x_i} \right\rangle + \left\langle \overline{\theta} \frac{\partial \overline{p}}{\partial x_i} - \overline{\theta} \frac{\partial \overline{p}}{\partial x_i} \right\rangle \right) \\ &\quad - \frac{\partial}{\partial x_3} (\langle \overline{u}_3'' \overline{u}_i'' \overline{\theta}'' \rangle + \langle \overline{u}_3'' \tau_{i\theta}'' \rangle + \langle \overline{u}_i'' \tau_{3\theta}'' \rangle + \langle \overline{\theta}'' \tau_{i3}'' \rangle + \langle \mathcal{T}_{3i\theta} \rangle), \end{aligned} \quad (9)$$

where $i = 1$ and $i = 2$ for the streamwise and the spanwise components of the temperature flux, respectively, and $\mathcal{T}_{3i\theta} = u_3 u_i \theta + 2 \overline{u}_3 \overline{u}_i \overline{\theta} - \overline{u}_3 \overline{u}_i \overline{\theta} - \overline{u}_3 u_i \theta - \overline{u}_i \theta u_3$ is the third-order SGS transport term. The terms on the rhs of Eq. (9) represent the effects of the mean temperature gradient, mean velocity shear, reference-frame rotation (Coriolis),

pressure gradient–temperature covariance, and turbulent transport, respectively. The SGS pressure-scrambling term is computed as (Heinze et al. 2015) $\langle \theta \partial p / \partial x_i - \theta \partial \overline{p} / \partial x_i \rangle = -\langle \tau_{k\theta} \partial \overline{u}_i / \partial x_k \rangle - \langle \tau_{ik} \partial \overline{\theta} / \partial x_k \rangle - \varepsilon_{i3k} f_3 \langle \tau_{k\theta} \rangle$. The SGS triple correlation term $\langle \mathcal{T}_{3i\theta} \rangle$ cannot be estimated from our LES data and is treated as part of the budget imbalance.

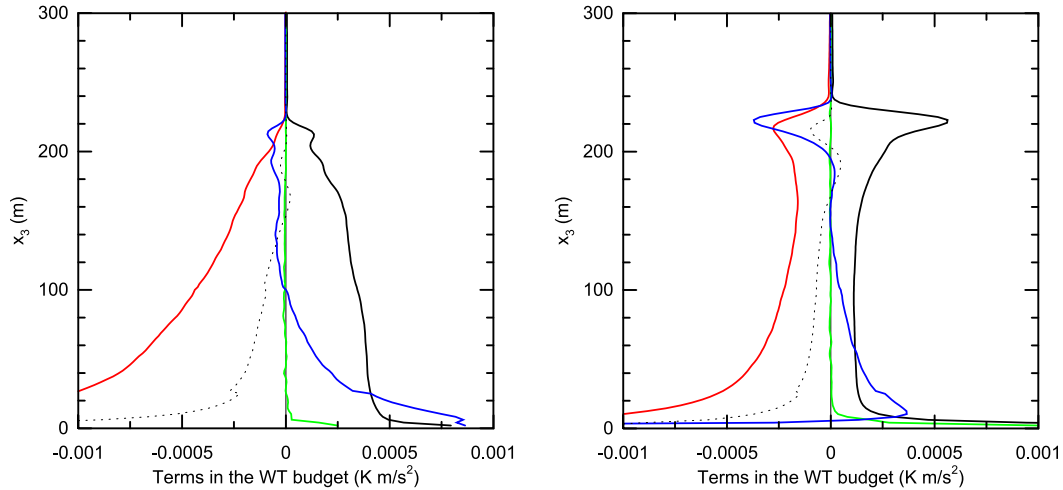


FIG. 7. Budget of the vertical temperature flux from simulations (left) HOM and (right) HET. Curves represent the effects of mean temperature gradient (red), buoyancy (black), pressure gradient–temperature covariance (blue), and third-order transport (green). Thin dotted black curves show the budget imbalance.

b. Budgets of TKE, vertical temperature flux, and temperature variance

The budgets of the $TKE = (1/2)\langle \bar{u}_i'^2 \rangle + \langle e \rangle$, of the vertical component of the temperature flux $WT = \langle \bar{u}_3' \bar{\theta}'' \rangle + \langle \tau_{3\theta} \rangle$, and of the temperature variance $TT = \langle \bar{\theta}''^2 \rangle + \langle \vartheta \rangle$ from simulations HOM and HET are shown in Figs. 6–8. The budget imbalance is computed as the sum of terms on the rhs of Eqs. (6)–(8). In all budgets, the imbalance is small as compared to the leading-order terms but is not entirely negligible. Notice, however, that turbulence in our SBL flows is never in a perfectly steady state. Continuous decrease of the surface temperature causes continuous adjustment of the SBL turbulence structure to changing static stability. Then the tendencies of TKE, WT, and TT are likely to contribute to the imbalance of the respective budget.

The TKE budgets from simulations HOM and HET are shown in Fig. 6. In both cases, the budget is dominated by the mean velocity shear and the dissipation terms. The transport term is small over most of the SBL, except close to the surface. The major difference between the two budgets is in the buoyancy flux [the second term on the rhs of Eq. (7)]. In the heterogeneous case, its magnitude is substantially reduced.

The budget of the vertical temperature flux, Fig. 7, is maintained by the mean temperature gradient term, the buoyancy term, and the pressure gradient–temperature covariance. The turbulent transport term is small, except in the close vicinity of the surface in HET. The major difference between HOM and HET is in the buoyancy term. In the heterogeneous case, it has a pronounced maximum near the SBL top, and, most notably, it is very large near the surface.

The largest difference between HOM and HET is exhibited by the temperature variance budget, Fig. 8. In the heterogeneous case, the amplitude of the mean-gradient and the dissipation terms is reduced in mid-SBL, apparently because of a reduced mean temperature gradient and, hence, a reduced variance production. The vertical flux of temperature variance is zero at the surface and at the SBL top in the homogeneous case. Hence, the turbulent transport term [the last term on the rhs of Eq. (6)], that is, the divergence of the third-order flux, acts to redistribute the temperature variance in the vertical. It integrates to zero over the entire SBL. In the heterogeneous case, the transport term does not integrate to zero and is a net gain of temperature variance. This is only possible if the flux of temperature variance is nonzero at the surface.

The expression for the vertical flux of temperature variance reads [see Eq. (6)]

$$\langle \bar{u}_3' \bar{\theta}''^2 \rangle + \langle \bar{u}_3' \vartheta'' \rangle + 2\langle \bar{\theta}'' \tau_{3\theta}'' \rangle + \langle T_{3\theta} \rangle. \quad (10)$$

The last term in Eq. (10) cannot be estimated from our LES but is most likely small (cf. Deardorff 1974a). The first two terms are zero at the surface because of zero vertical velocity \bar{u}_3 . The third term is zero in HOM since the surface is homogeneous with respect to the temperature $\bar{\theta}$. This is not the case in HET, where the surface temperature varies in the streamwise direction. Surface temperature variations modify local stability conditions, thus modulating the surface temperature flux so that $\bar{\theta}$ and $\tau_{3\theta}$ are correlated. Positive fluctuations of temperature about its horizontal mean, $\bar{\theta}'' > 0$, reduce local temperature gradient, leading to a reduced

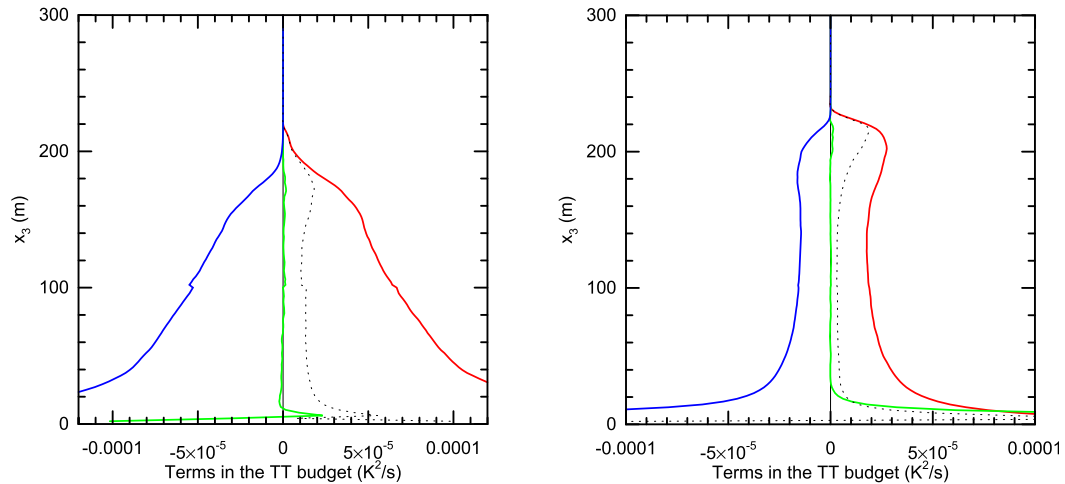


FIG. 8. The temperature variance budget from simulations (left) HOM and (right) HET. Curves represent the effects of mean temperature gradient (red), dissipation (blue), and third-order transport (green). Thin dotted black curves show the budget imbalance.

magnitude of the downward (negative) temperature flux (the local flux can even become positive), that is, $\tau_{3\theta}'' > 0$. And vice versa, negative temperature fluctuations, $\bar{\theta}'' < 0$, increase the local temperature gradient, leading to $\tau_{3\theta}'' < 0$. Then, $\bar{\theta}$ and $\tau_{3\theta}$ are positively correlated, leading to a positive temperature variance flux at the surface. It should be stressed that this result cannot be obtained if the third-order moment (flux of

temperature variance) is estimated on the basis of resolved-scale fields only, that is, keeping only the first term in Eq. (10).

The above analysis suggests the following qualitative explanation of enhanced vertical mixing in the SBL over a thermally heterogeneous surface. As a result of heterogeneity, the temperature variance near the surface strongly increases. The temperature variance

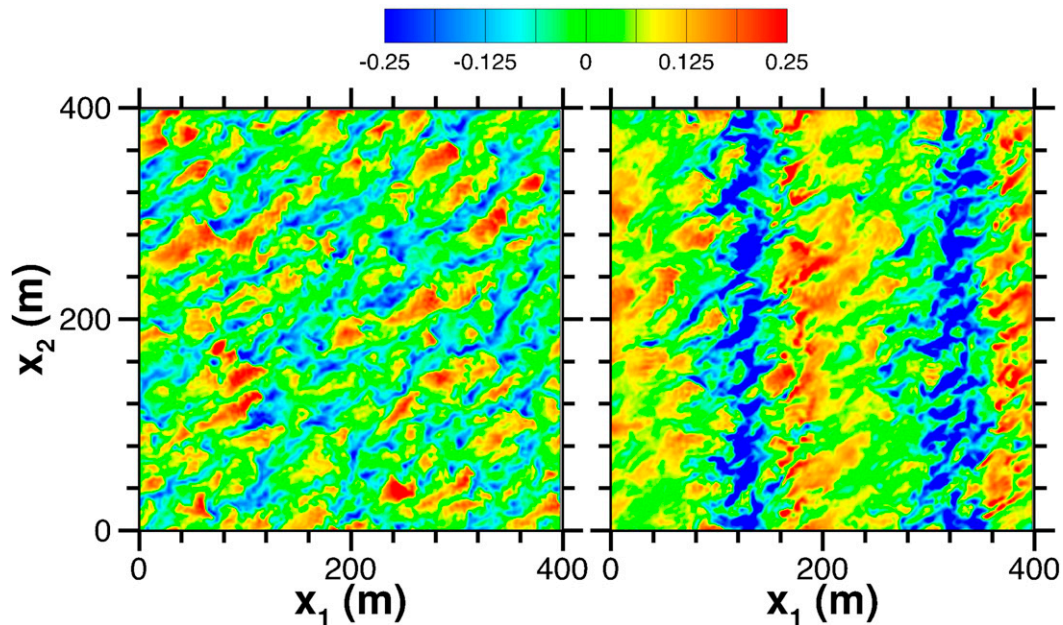


FIG. 9. Horizontal cross sections of the fluctuations of potential temperature about its horizontal mean (K) for simulations (left) HOM and (right) HET. The cross sections are taken at $x_3 = 3.125$ m above the ground near the end of the sampling period (simulation time is 35 000 s). Red (blue) colors correspond to positive (negative) values of the temperature fluctuation, as shown in the color scale bar.

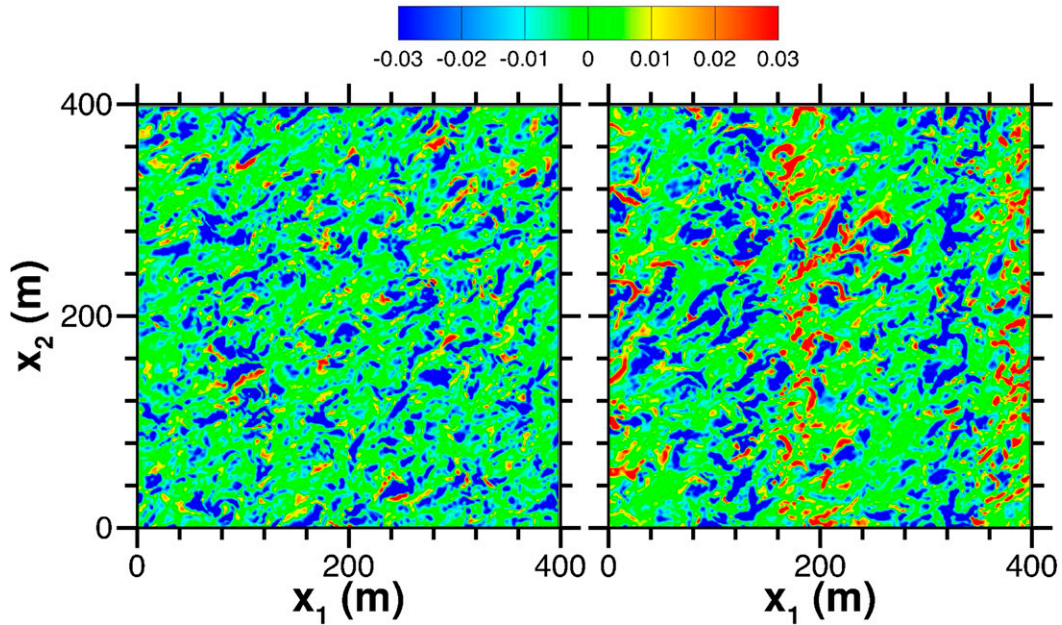


FIG. 10. Horizontal cross sections of the resolved-scale vertical temperature flux (K m s^{-1}) for simulations (left) HOM and (right) HET. The cross sections are taken at $x_3 = 4.167$ m above the ground near the end of the sampling period (simulation time is 35 000 s). Red (blue) colors correspond to positive (negative) values of the temperature flux, as shown in the color scale bar.

multiplied by the buoyancy parameter enters the vertical temperature flux budget, Eq. (8), as the buoyancy production term. As it acts to generate a positive (upward) temperature flux, an increased temperature variance partially compensates the mean-gradient term that acts to generate a negative (downward) temperature flux. As a result, the downward temperature flux is reduced in magnitude. Because in a quasi-steady SBL the vertical temperature flux is nearly linear (see Fig. 2), a reduction occurs not only near the surface but also over most of the SBL. In stable stratification, the buoyancy flux (temperature flux times the buoyancy parameter) is the sink term in the TKE budget, Eq. (7). A reduced magnitude of the buoyancy flux means that less energy is spent working against gravity, leading to an increased TKE (note that both horizontal and vertical velocity variances are increased; see Fig. 4) and more vigorous vertical mixing in the heterogeneous SBL as compared to its homogeneous counterpart.

The effect of surface temperature heterogeneity is further visualized in Figs. 9 and 10. Figure 9 shows fluctuations of potential temperature about its horizontal mean $\bar{\theta}''$ in an x_1 - x_2 plane just above the underlying surface. We readily observe organized cold and warm stripes phase locked to the underlying surface in the heterogeneous case. The resolved-scale vertical temperature flux $\overline{w''\theta''}$ shown in Fig. 10 is predominantly

negative (downward) in the homogeneous case. In the heterogeneous case, two stripes of positive $\overline{w''\theta''}$ are clearly seen, the locations of which roughly correspond to the locations of stripes of positive $\bar{\theta}''$ shown in Fig. 9 (right). Advection of cold air over a warm surface results in a negative vertical temperature gradient (cf. Stoll and Porté-Agel 2009) that generates positive (upward) temperature flux over quite extended regions of the flow (two red stripes in Fig. 10, right). The flow in the heterogeneous case remains stably stratified in a global (horizontal mean) sense, but the magnitude of the downward temperature flux (Fig. 2), and hence of the buoyancy flux (Fig. 6), is reduced as compared to the homogeneous case, leading to more vigorous vertical mixing in the heterogeneous SBL.

It should be noted that, in the heterogeneous case, the transport term in the WT budget does not integrate to zero and is a net source (sink) of the vertical temperature flux. This effect can be explained in a similar fashion as the effect of the temperature variance production by the third-order correlation, the divergence of which enters the vertical temperature flux budget, Eq. (8), reads

$$\langle \overline{u_3''^2 \theta''} \rangle + 2 \langle \overline{u_3'' r_{3\theta}''} \rangle + \langle \overline{\theta'' r_{33}''} \rangle + \langle \mathcal{T}_{33\theta} \rangle. \quad (11)$$

The last term in Eq. (11) cannot be estimated from our LES but is most likely small, and the first two terms are

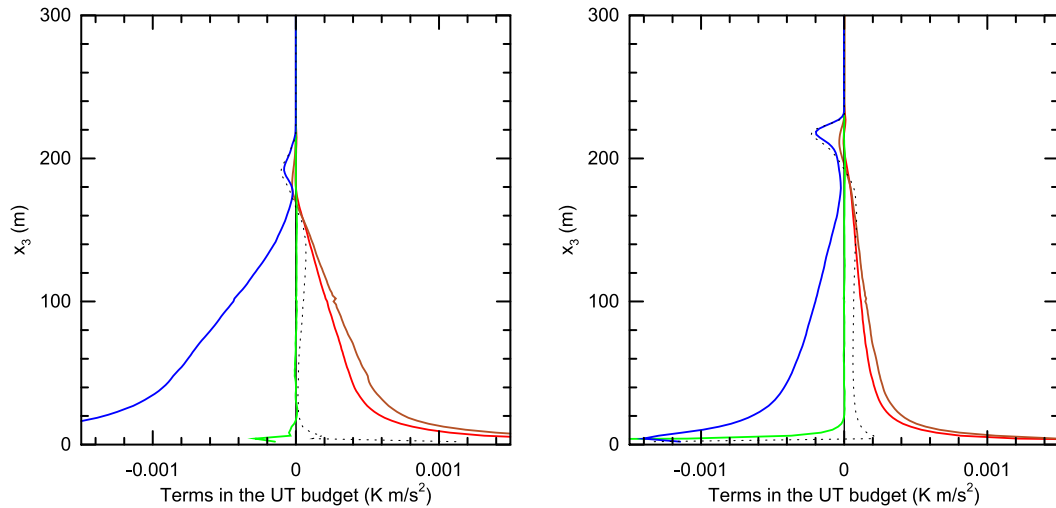


FIG. 11. Budget of the streamwise component of the temperature flux from simulations (left) HOM and (right) HET. Curves represent the effects of mean temperature gradient (red), mean velocity shear (brown), pressure gradient–temperature covariance (blue), third-order transport (green), and reference-frame rotation (black, closely following zero). Thin dotted black curves show the budget imbalance.

zero at the surface because of zero vertical velocity. The single remaining term is zero in HOM but nonzero in HET, where the surface temperature variations change local stability conditions and modulate the surface Reynolds stress components. In HET, $\bar{\theta}$ and τ_{33} prove to be positively correlated, thus contributing to the production of positive (upward) temperature flux. That is, near the surface, the effect of the third-order term in the WT budget in the heterogeneous SBL is analogous to the effect of the buoyancy term. Both terms generate a positive (upward) temperature flux that partially compensates for a negative (downward) temperature flux produced by the mean temperature gradient. However, the buoyancy effect is stronger because of a drastic increase of the temperature variance near the thermally heterogeneous surface. It is this increase of TT that should be primarily accounted for to parameterize the effect of the surface temperature heterogeneity on the SBL mean and turbulence structure.

c. Budgets of horizontal temperature flux components

The budgets of the streamwise $UT = \langle \bar{u}_1'' \bar{\theta}'' \rangle + \langle \tau_{1\theta} \rangle$ and spanwise $VT = \langle \bar{u}_2'' \bar{\theta}'' \rangle + \langle \tau_{2\theta} \rangle$ components of the temperature flux from simulations HOM and HET are shown in Figs. 11 and 12, respectively. In both HOM and HET, the budgets of UT and VT are maintained by the mean temperature gradient and the mean velocity shear terms (sources), as well as the pressure gradient–temperature covariance (sink). The amplitude of these leading-order terms is smaller in the heterogeneous case than in the homogeneous case. This occurs because of reduced gradients of mean temperature and mean

velocity (see Fig. 1) and, hence, a reduced flux production. The Coriolis terms are negligibly small in both HOM and HET. The turbulent transport terms are small in both cases over most of the SBL, except near the surface in HET. In the heterogeneous case, the transport terms do not integrate to zero and are a net gain to the horizontal components of the temperature flux (note that this flux budget term is a source and has the same sign as the flux itself; also UT and VT are negative near the surface in the heterogeneous case, Fig. 3). This effect can be explained in a similar way as the effect of the temperature variance and the vertical temperature flux production by the third-order terms in the heterogeneous SBL (section 4b).

Consider the expression for the third-order velocity–temperature correlation (loosely referred to as the “flux of temperature flux”), the divergence of which enters the horizontal temperature flux budget, Eq. (9). It reads

$$\langle \bar{u}_3'' \bar{u}_i'' \bar{\theta}'' \rangle + \langle \bar{u}_3'' \tau_{i\theta}'' \rangle + \langle \bar{u}_i'' \tau_{3\theta}'' \rangle + \langle \bar{\theta}'' \tau_{i3}'' \rangle + \langle T_{3i\theta} \rangle, \quad (12)$$

where $i = 1$ and $i = 2$ for UT and VT, respectively. The last term in Eq. (12) cannot be estimated from our LES but is most likely small. The first three terms are zero at the surface as a result of zero mean velocity, $\bar{u}_1 = \bar{u}_2 = \bar{u}_3 = 0$. The single remaining term is zero in HOM since the surface is thermally homogeneous. In HET, the surface temperature varies. Surface temperature variations change local stability conditions, thus modulating the surface momentum flux components. As a result, $\bar{\theta}$ and τ_{i3} prove to be correlated. Positive temperature fluctuations (about the horizontal-mean

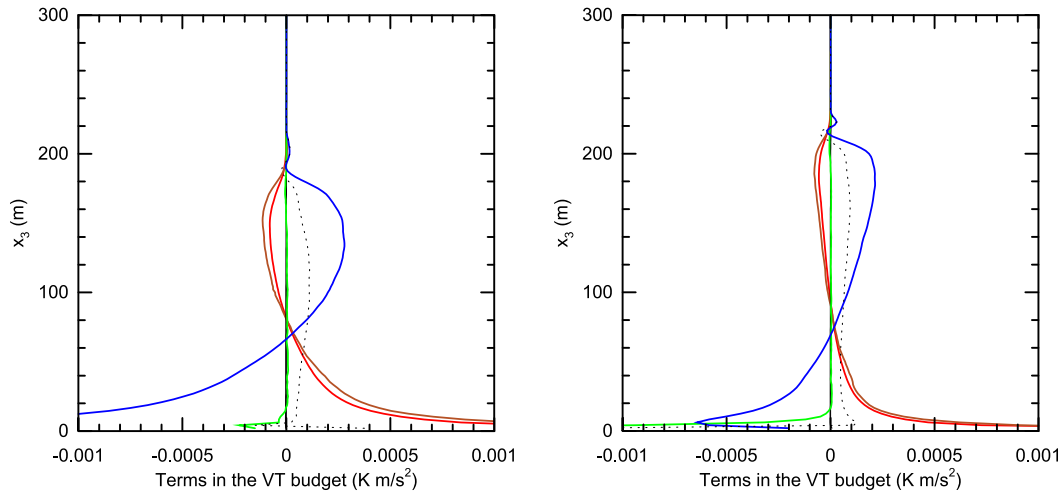


FIG. 12. Budget of the spanwise component of the temperature flux from simulations (left) HOM and (right) HET. Curves represent the effects of mean temperature gradient (red), mean velocity shear (brown), pressure gradient–temperature covariance (blue), third-order transport (green), and reference-frame rotation (black, closely following zero). Thin dotted black curves show the budget imbalance.

temperature), $\overline{\theta''} > 0$, reduce the local temperature gradient and, hence, local static stability, leading to an enhanced momentum transport toward the surface, that is, $\tau''_{13} < 0$ and $\tau''_{23} < 0$. And vice versa, negative temperature fluctuations, $\overline{\theta''} < 0$, increase the local static stability, leading to a reduced momentum transport toward the surface, that is, $\tau''_{13} > 0$ and $\tau''_{23} > 0$. Then, $\overline{\theta}$ and τ_{i3} ($i = 1$ for UT and $i = 2$ for VT) are negatively correlated, leading to a negative surface flux of the horizontal temperature flux components. It should be stressed (cf. the discussion of TT and WT budgets in section 4b) that this result cannot be obtained if the third-order moment is estimated on the basis of resolved-scale fields only, that is, keeping only the first term in Eq. (12).

5. Discussion

The above analysis suggests a key role of the temperature variance in turbulent mixing in a horizontally heterogeneous SBL. To incorporate the effect of surface temperature heterogeneity, SBL turbulence models (parameterization schemes) should account for an increased temperature variance near the surface. Proper allowance should also be made for nonzero third-order transport terms in the temperature variance and temperature flux budgets. Unfortunately, turbulence closures applied to the entire SBL not only should account for the above effects (e.g., through the use of temperature variance transport equation with a physically sound parameterization of the third-order moment), but also the surface-layer flux–profile relationships should be modified accordingly. This notoriously difficult task is beyond the scope of the present study.

As a first approximation, the effect of the surface temperature heterogeneity can be accounted for by utilizing a tile approach that is widely used in atmospheric models (e.g., Avissar and Pielke 1989; Giorgi and Avissar 1997; Moene and van Dam 2014, and references therein). The basic idea is to couple the SBL turbulence closure scheme with a tiled surface scheme, where several homogeneous parts with different surface temperatures are considered within a host model grid box and conventional surface-layer flux–profile relationships are applied to each part. Modified flux–profile relationships developed by Stoll and Porté-Agel (2009) on the basis of local similarity theory hold some promise. Despite its shortcomings, the tile approach is a reasonable option from a practical standpoint (at least to a first approximation). Efforts are being made (E. Machulskaya 2015, personal communication) to couple a tiled surface scheme with a two-equation turbulence model, which carries transport equations for both the TKE and the temperature variance (Machulskaya and Mironov 2013). The coupling raises a number of issues, for example, the formulation of the lower boundary condition for the temperature variance, where both the temperature difference between various surface tiles and the nonzero surface value of the third-order velocity–temperature correlation should be taken into account.

A word of caution about the fidelity of LES as applied to the SBL is in order. Since turbulence in the SBL is dominated by small-scale eddies, and turbulent transport in most of the boundary layer essentially depends on the heat and momentum transfer near the surface,

one may argue that an LES of SBL is uncertain, except perhaps when the resolution is extremely high (as, e.g., in Sullivan et al. 2015, manuscript submitted to *J. Atmos. Sci.*). The argument is valid, and caution is indeed required when interpreting LES data on stably stratified flows. We believe, however, that our findings are broadly independent of possible LES uncertainties. For example, the third-order moment in the temperature variance budget is large at the surface in the simulation HET and is zero in the simulation HOM. That is, we do not attempt to scrutinize a small difference of two large quantities; rather, we compare quantities whose magnitudes are drastically different. Hence, the results should be qualitatively reliable, although the estimates of various turbulent quantities derived from LES may be somewhat uncertain in a quantitative sense.

One more issue related to the heterogeneous flows is the applicability of surface-layer flux–profile relationships in the LES. Sullivan et al. (1994) proposed an SGS model where the horizontal-mean momentum and temperature fluxes and the horizontal-mean profiles of velocity and temperature are forced to obey the Monin–Obukhov surface-layer similarity (see also Stoll and Porté-Agel 2006). As the Monin–Obukhov surface-layer flux–profile relationships are applicable to continuous turbulence over a homogeneous surface, it would be incorrect to enforce the Monin–Obukhov similarity in the horizontal-mean sense over a thermally heterogeneous surface. We therefore apply the surface-layer relationships locally, that is, point by point in the LES (cf. Stoll and Porté-Agel 2009). On the other hand, the Monin–Obukhov similarity deals with the ensemble-mean quantities. Since turbulence near the surface is small scale, a grid volume between the surface and the first model level above may contain a large enough ensemble of turbulent eddies, which effectively makes a grid-volume mean a fair approximation to the ensemble mean. This is not a priori clear, however, so some uncertainties remain. A possible way to improve the situation is to apply the surface-layer relationships to the quantities averaged over $n \times n$ grid points. The value of n should be chosen (by trial and error, unless sound theoretical arguments can be adduced) to provide a good approximation to the ensemble-mean quantities but should still be small enough to avoid detectable surface heterogeneity within the area of $n \times n$ grid points. A detailed consideration of the surface-layer similarity as applied in LES of flows with heterogeneous underlying surface is beyond the scope of the present study. It should be a subject for future work.

It should be recognized that our results are pertinent to the SBL with weak-to-moderate static stability. Although the cases HOM and HET are different in terms

of the intensity of mixing, turbulence in both cases is well developed. In the future, strongly stable boundary layers need to be investigated, where turbulence over a homogeneous surface tends to die out (cf. Nieuwstadt 2005; Flores and Riley 2011; Ansorge and Mellado 2014). A key question is whether turbulence survives over a heterogeneous surface and, if so, whether it generates appreciable vertical fluxes of momentum and heat. The behavior of other turbulence statistics in a strongly stable regime is also of considerable interest, for example, if the surface flux of temperature variance remains positive. LES may not be an appropriate tool to study strongly stable regimes. DNS seems to be an appropriate alternative, at least to obtain qualitative answers to the above questions.

One more important issue is the dependence of the SBL mean and turbulence structure on the size of the surface heterogeneity patterns. Stoll and Porté-Agel (2009) found that the magnitude of the temperature difference between the warm and the cold stripes has a pronounced effect on the SBL structure, whereas the results proved to be practically independent of the number of cold and warm stripes. We chose a configuration with two warm stripes and two cold stripes. Test runs with a different number of warm and cold stripes (not shown) corroborate the finding of Stoll and Porté-Agel (2009). Recall that the flows in simulations of Stoll and Porté-Agel (2009) and in our simulations are in the weakly stable regime. Although the flows are stably stratified in a global (horizontal mean) sense, the vertical temperature gradient near the surface is negative in some regions of the flow. Because of the advection of cold air over a warm surface, convective instability develops locally, and convective vortices are formed. It is in this weakly stable regime that the results appear to be practically independent of the number of stripes and, hence, of the size of the stripes relative to the domain size (at least for the SBL depths and heterogeneity sizes used in our runs and in the runs performed by Stoll and Porté-Agel). In strongly stable boundary layers, where the flow is statically stable (almost) everywhere, turbulence is likely to be affected by internal gravity waves rather than vortices as in a weakly stable regime. Then it cannot be stated a priori that the SBL mean and turbulence structure would be grossly independent of the size of the surface heterogeneity patterns. Investigation of this issue should be a subject for future work.

6. Conclusions

Idealized LES of two SBL flows driven by fixed winds and homogeneous and heterogeneous surface temperature are compared. The LES data are used to compute

statistical moments of the fluctuating fields (mean wind and mean potential temperature, second-order and third-order turbulence moments, and pressure–velocity and pressure–scalar covariances), to estimate terms in the second-moment budgets, and to assess the relative importance of various terms in maintaining the budgets. The budgets of TKE, of the temperature variance, and of the vertical and horizontal components of the temperature flux are analyzed. Unlike most previous studies, the LES-based second-moment budgets are estimated with due regard for the subgrid-scale contributions. These contributions may be substantial even at high resolution, particularly in the SBL, and should be retained in order to close the second-moment budgets to a good order.

We find the SBL over a heterogeneous surface is more turbulent with larger TKE, is better vertically mixed, and is deeper compared to its homogeneous counterpart. The most striking difference between the homogeneous and heterogeneous cases is exhibited by the temperature variance and its budget. Because of surface heterogeneity, the temperature variance is very large near the surface in the heterogeneous SBL. The third-order moment, that is, the vertical flux of temperature variance, is non-zero at the surface. Hence, the turbulent transport term (divergence of the above third-order moment) not only redistributes the temperature variance in the vertical but is a net gain. An increase in the temperature variance near the surface helps explain a reduced magnitude of the downward temperature flux and more vigorous mixing in the heterogeneous case.

Analysis of the temperature flux budget shows that the transport term (divergence of the third-order moment) does not integrate to zero over the heterogeneous SBL. Because of a nonzero third-order velocity–temperature correlation at the surface, the transport term appears to be a net source (sink) of the temperature flux component in question, just as the transport term is a net source in the temperature variance budget. It is emphasized that this result cannot be obtained if the temperature variance and temperature flux budgets are estimated on the basis of resolved-scale fields only, that is, the SGS contributions to the budget terms are neglected.

Our analysis suggests a key role of the temperature variance in turbulent mixing in a horizontally heterogeneous SBL. Turbulence models (parameterization schemes) suitable for a horizontally heterogeneous SBL should account for an increased temperature variance near the surface and should make proper allowance for nonzero third-order transport terms in the temperature variance and temperature flux budgets. Importantly, not only turbulence closures applied to the SBL interior but also the surface-layer flux–profile relationships should

account for the above effects. Development of such formulations should be a subject for future work. As a rough approximation, the effect of the surface temperature heterogeneity can be accounted for by coupling a turbulence closure model with a tiled surface scheme, where several homogeneous tiles with different surface temperatures are considered and conventional surface-layer flux–profile relationships are applied to each tile.

Note finally that our results are pertinent to the SBL with weak-to-moderate static stability. Future efforts should focus on the analysis of mean and turbulence structure of a strongly stable boundary layer over thermally heterogeneous surfaces. LESs of strongly stable flows with laminar-turbulent transitions are uncertain because of the SGS parameterizations. Strongly stable flows are perhaps more appropriately modeled using DNS.

Acknowledgments. We thank Vittorio Canuto, Sergey Danilov, Evgeni Fedorovich, Vladimir Gryanik, Donald Lenschow, Ekaterina Machulskaya, Chin-Hoh Moeng, Ned Patton, Matthias Raschendorfer, and Jeffrey Weil for useful discussions. Comments of the reviewers Chiel van Heerwaarden, Evgeni Fedorovich, and Juan Pedro Mellado helped to improve the manuscript. The work was partially supported by the NCAR Geophysical Turbulence Program and by the European Commission through the COST Action ES0905.

REFERENCES

- Andr n, A., 1995: The structure of stably stratified atmospheric boundary layers: A large-eddy simulation study. *Quart. J. Roy. Meteor. Soc.*, **121**, 961–985, doi:10.1002/qj.49712152502.
- Ansonge, C., and J. P. Mellado, 2014: Global intermittency and collapsing turbulence in the stratified planetary boundary layer. *Bound.-Layer Meteor.*, **153**, 89–116, doi:10.1007/s10546-014-9941-3.
- Avissar, R., and R. A. Pielke, 1989: A parameterization of heterogeneous land surfaces for atmospheric numerical models and its impact on regional meteorology. *Mon. Wea. Rev.*, **117**, 2113–2136, doi:10.1175/1520-0493(1989)117<2113: APOHLS>2.0.CO;2.
- Beare, R. J., and Coauthors, 2006: An intercomparison of large-eddy simulations of the stable boundary layer. *Bound.-Layer Meteor.*, **118**, 247–272, doi:10.1007/s10546-004-2820-6.
- Brown, A. R., S. H. Derbyshire, and P. J. Mason, 1994: Large-eddy simulation of stable atmospheric boundary layers with a revised stochastic subgrid model. *Quart. J. Roy. Meteor. Soc.*, **120**, 1485–1512, doi:10.1002/qj.49712052004.
- Coleman, G. N., J. H. Ferziger, and P. R. Spalart, 1992: Direct simulation of the stably stratified turbulent Ekman layer. *J. Fluid Mech.*, **244**, 677–712, doi:10.1017/S0022112092003264.
- Deardorff, J. W., 1973: The use of subgrid transport equations in a three-dimensional model of atmospheric turbulence. *J. Fluids Eng.*, **95**, 429–438, doi:10.1115/1.3447047.
- , 1974a: Three-dimensional numerical study of the height and mean structure of a heated planetary boundary layer. *Bound.-Layer Meteor.*, **7**, 81–106, doi:10.1007/BF00224974.

- , 1974b: Three-dimensional numerical study of turbulence in an entraining mixed layer. *Bound.-Layer Meteor.*, **7**, 199–226, doi:10.1007/BF00227913.
- , 1980: Stratocumulus-capped mixed layers derived from a three-dimensional model. *Bound.-Layer Meteor.*, **18**, 495–527, doi:10.1007/BF00119502.
- Flores, O., and J. J. Riley, 2011: Analysis of turbulence collapse in the stably stratified surface layer using direct numerical simulation. *Bound.-Layer Meteor.*, **139**, 241–259, doi:10.1007/s10546-011-9588-2.
- Giorgi, F., and R. Avissar, 1997: Representation of heterogeneity effects in Earth system modeling: Experience from land surface modeling. *Rev. Geophys.*, **35**, 413–438, doi:10.1029/97RG01754.
- Heinze, R., D. Mironov, and S. Raasch, 2015: Second-moment budgets in cloud-topped boundary layers: A large-eddy simulation study. *J. Adv. Model. Earth Syst.*, **7**, 510–536, doi:10.1002/2014MS000376.
- Huang, J., and E. Bou-Zeid, 2013: Turbulence and vertical fluxes in the stable atmospheric boundary layer. Part I: A large-eddy simulation study. *J. Atmos. Sci.*, **70**, 1513–1527, doi:10.1175/JAS-D-12-0167.1.
- Jiménez, M. A., and J. Cuxart, 2005: Large-eddy simulations of the stable boundary layer using the standard Kolmogorov theory: Range of applicability. *Bound.-Layer Meteor.*, **115**, 241–261, doi:10.1007/s10546-004-3470-4.
- Khanna, S., 1998: Comparison of Kansas data with high-resolution large-eddy simulation fields. *Bound.-Layer Meteor.*, **88**, 121–144, doi:10.1023/A:1001068612129.
- Kosović, B., and J. A. Curry, 2000: A large-eddy simulation study of a quasi-steady, stably stratified atmospheric boundary layer. *J. Atmos. Sci.*, **57**, 1052–1068, doi:10.1175/1520-0469(2000)057<1052:ALESSO>2.0.CO;2.
- Lilly, D. K., 1967: The representation of small-scale turbulence in numerical simulation experiments. *Proc. IBM Scientific Computing Symp. on Environmental Sciences*, IBM Form 320-1951, Yorktown Heights, NY, International Business Machines Corporation, 195–210.
- Machulskaya, E., and D. Mironov, 2013: Implementation of TKE–scalar variance mixing scheme into COSMO. *COSMO Newsletter*, No. 13, Consortium for Small-Scale Modeling, 25–33.
- Mahrt, L., 2014: Stably stratified atmospheric boundary layers. *Annu. Rev. Fluid Mech.*, **46**, 23–45, doi:10.1146/annurev-fluid-010313-141354.
- Mason, P. J., and S. H. Derbyshire, 1990: Large-eddy simulation of the stably-stratified atmospheric boundary layer. *Bound.-Layer Meteor.*, **53**, 117–162, doi:10.1007/BF00122467.
- Mironov, D. V., 2001: Pressure–potential-temperature covariance in convection with rotation. *Quart. J. Roy. Meteor. Soc.*, **127**, 89–110, doi:10.1002/qj.49712757106.
- , 2009: Turbulence in the lower troposphere: Second-order closure and mass–flux modelling frameworks. *Interdisciplinary Aspects of Turbulence*, W. Hillebrandt and F. Kupka, Eds., Lecture Notes in Physics, Vol. 756, Springer-Verlag, 161–221, doi:10.1007/978-3-540-78961-1_5.
- , V. M. Gryanik, C.-H. Moeng, D. J. Olbers, and T. H. Warncke, 2000: Vertical turbulence structure and second-moment budgets in convection with rotation: A large-eddy simulation study. *Quart. J. Roy. Meteor. Soc.*, **126**, 477–515, doi:10.1002/qj.49712656306.
- Moene, A. F., and J. C. van Dam, 2014: *Transport in the Atmosphere–Vegetation–Soil Continuum*. Cambridge University Press, 436 pp.
- Moeng, C.-H., 1984: A large-eddy-simulation model for the study of planetary boundary-layer turbulence. *J. Atmos. Sci.*, **41**, 2052–2062, doi:10.1175/1520-0469(1984)041<2052:ALESMF>2.0.CO;2.
- , and J. C. Wyngaard, 1988: Spectral analysis of large-eddy simulations of the convective boundary layer. *J. Atmos. Sci.*, **45**, 3573–3587, doi:10.1175/1520-0469(1988)045<3573:SAOLES>2.0.CO;2.
- Moeng, C. H., and J. C. Wyngaard, 1989: Evaluation of turbulent transport and dissipation closures in second-order modeling. *J. Atmos. Sci.*, **46**, 2311–2330, doi:10.1175/1520-0469(1989)046<2311:EOTTAD>2.0.CO;2.
- Nieuwstadt, F. T. M., 2005: Direct numerical simulation of stable channel flow at large stability. *Bound.-Layer Meteor.*, **116**, 277–299, doi:10.1007/s10546-004-2818-0.
- , P. J. Mason, C. H. Moeng, and U. Schumann, 1993: Large-eddy simulation of the convective boundary layer: A comparison of four computer codes. *Turbulent Shear Flows 8*, F. Durst et al., Eds., Springer-Verlag, 343–367, doi:10.1007/978-3-642-77674-8_24.
- Peltier, L. J., and J. C. Wyngaard, 1995: Structure–function parameters in the convective boundary layer from large-eddy simulation. *J. Atmos. Sci.*, **52**, 3641–3660, doi:10.1175/1520-0469(1995)052<3641:SPITCB>2.0.CO;2.
- Pope, S. B., 2000: *Turbulent Flows*. Cambridge University Press, 771 pp.
- Saiki, E. M., C.-H. Moeng, and P. P. Sullivan, 2000: Large-eddy simulation of the stably stratified planetary boundary layer. *Bound.-Layer Meteor.*, **95**, 1–30, doi:10.1023/A:1002428223156.
- Stoll, R., and F. Porté-Agel, 2006: Effect of roughness on surface boundary conditions for large-eddy simulation. *Bound.-Layer Meteor.*, **118**, 169–187, doi:10.1007/s10546-005-4735-2.
- , and —, 2009: Surface heterogeneity effects on regional-scale fluxes in stable boundary layers: Surface temperature transitions. *J. Atmos. Sci.*, **66**, 412–431, doi:10.1175/2008JAS2668.1.
- Sullivan, P. P., and E. G. Patton, 2008: A highly parallel algorithm for turbulence simulations in planetary boundary layers: Results with meshes up to 1024³. *18th Symp. on Boundary Layers and Turbulence*, Stockholm, Sweden, Amer. Meteor. Soc., 11B.5. [Available online at https://ams.confex.com/ams/18BLT/techprogram/paper_139870.htm.]
- , and —, 2011: The effect of mesh resolution on convective boundary layer statistics and structures generated by large-eddy simulation. *J. Atmos. Sci.*, **68**, 2395–2415, doi:10.1175/JAS-D-10-05010.1.
- , J. C. McWilliams, and C.-H. Moeng, 1994: A subgrid-scale model for large-eddy simulation of planetary boundary-layer flows. *Bound.-Layer Meteor.*, **71**, 247–276, doi:10.1007/BF00713741.
- , —, and —, 1996: A grid nesting method for large-eddy simulation of planetary boundary-layer flows. *Bound.-Layer Meteor.*, **80**, 167–202, doi:10.1007/BF00119016.
- Taylor, J. R., and S. Sarkar, 2008: Stratification effects in a bottom Ekman layer. *J. Phys. Oceanogr.*, **38**, 2535–2555, doi:10.1175/2008JPO3942.1.
- van Dop, H., and S. Axelsen, 2007: Large eddy simulation of the stable boundary-layer: A retrospect to Nieuwstadt’s early work. *Flow Turbul. Combust.*, **79**, 235–249, doi:10.1007/s10494-007-9093-3.